applied sciences

MDPI

Article

Analysis of Coil Systems with Non-Symmetrical Fe Backings for Electrical Vehicle Wireless Charging Applications

Robertas Lukočius [1,*], Žilvinas Nakutis [2], Andrius Vilkauskas [3], Ramūnas Deltuva [1] and Lukas Romikaitis [1]

[1] Department of Electrical Power Systems, Faculty of Electrical and Electronics Engineering, Kaunas University of Technology, Studentų St. 48, 51367 Kaunas, Lithuania; ramunas.deltuva@ktu.lt (R.D.); lukas.romikaitis@ktu.edu (L.R.)
[2] Department of Electronics Engineering, Faculty of Electrical and Electronics Engineering, Kaunas University of Technology, Studentų St. 50, 51368 Kaunas, Lithuania; zilvinas.nakutisl@ktu.lt
[3] Faculty of Mechanical Engineering and Design, Kaunas University of Technology, Studentų St. 56, 51424 Kaunas, Lithuania; andrius.vilkauskas@ktu.lt
* Correspondence: robertas.lukocius@ktu.lt

Abstract: Wireless power transfer is a widely applied technology whose market and application areas are growing rapidly. It is considered to be a promising supplement to the conductive charging of electrical vehicles (EVs). Wireless charging provides safety, convenience, and reliability in terms of mitigating issues related to wiring, risk of tearing, trip hazards, and contact wear inherent to the conductive charging. A variety of coil structures have been researched for EV charging applications; however, most of them were of the symmetrical type. This work analyzes systems of coils possessing ferromagnetic backing with non-symmetrical geometries and compares them with the conventional symmetrical ones. Numerical FEM simulation was applied in the research. The numerical models were verified analytically and experimentally. The impact of air-gap length, longitudinal displacement, number of turns, and width of the ferrite bars on coupling factor was investigated. The results suggest that coil systems with non-symmetrical structures of ferromagnetic backings are a good alternative to the conventional symmetrical structures for wireless electrical vehicle charging applications.

Keywords: electric vehicles; charging; wireless power transfer; ferromagnetic backings; coupling coefficient; finite element analysis

Citation: Lukočius, R.; Nakutis, Ž.; Vilkauskas, A.; Deltuva, R.; Romikaitis, L. Analysis of Coil Systems with Non-Symmetrical Fe Backings for Electrical Vehicle Wireless Charging Applications. *Appl. Sci.* **2024**, *14*, 1380. https://doi.org/10.3390/app14041380

Academic Editors: Chunhua Liu, Wei Han and Xiaoyang Tian

Received: 28 December 2023
Revised: 31 January 2024
Accepted: 1 February 2024
Published: 8 February 2024

1. Introduction

Wireless charging is a beneficial technology, removing the usage of cables and connectors, which finds its place in many practical application areas such as consumer electronics, medicine, healthcare, automotive, industrial, communications, aerospace, and defense industries. The wireless charging market is valued in the range of USD multi-billions and is expected to experience massive growth in this decade [1]. The growth is determined by the boost of the battery-powered devices market [1,2] and the development of methods and materials assuring high efficiency and affordability of the technology [3,4]. After starting from relatively low-power application areas such as consumer electronics, medicine, communications, and sensing, wireless charging also has spread towards high-power applications [5–7]. A huge potential for high-power wireless charging technology is found in automotive applications, especially for electric vehicle battery charging. As climate change demands that we switch to environmentally friendly technologies, vehicle manufacturers shift their focus from conventional internal-combustion-engine-powered vehicles towards electric ones [8]. The rapidly growing number of electrical vehicles demands widespread and handily applicable EV charging infrastructure development, correspondingly [9]. In addition to the primary purpose of EV batteries, to store energy for their operation, together

with acting as financially motivating tools, they are considered to be an additional tool helpful for the power balancing of electrical power systems [10–12]. Along with conventional conductive AC charging or DC off-board charging [13], wireless power charging appears to be an additional desirable option [14]. The nature of wireless chargers, allowing easy and safe [15,16] connection and disconnection from the power network, is compatible with the users' demands. Consequentially, the topic of wireless power transfer among researchers has recently been experiencing a renaissance.

One of the critical parameters determining the efficiency and power transfer capability of a WPT system is the coupling coefficient of the coupling coils [17]. In EV charging applications, the system must be capable of transferring high power with high efficiency through relatively large air-gaps [18]. Therefore, the analysis of the coupling coefficient of the coils' systems is receiving researchers' attention. A recently published wireless transferred power measurement method's error exhibited a dependence on the coupling coefficient, confirming its maximization benefits for accurate metering [19]. An optimization of the design is presented with respect to the coupling coefficient maximization of coil systems for EV charging applications by applying the finite element method in [20]. The focus of this work is set on research on ferrite saturation and its thickness optimization. A comparison of self and mutual inductances, as well as coupling factors of coils with circular and square geometries based on FEM analysis, is presented in [21]. The work presents an analysis of coreless structures, and core-based structures with and without aluminum shielding. However, different shape coupling systems with different numbers of ferrite bars and just the coil systems with symmetrical designs are compared in [21]. A method for magnetic structures for roadway WPT (Wireless Power Transfer) systems is proposed in [22]. The method is based on the simplified 2D finite element analysis of the coil systems. In [17], the influence of coil misalignment on coupling coefficient, mutual inductance, and quality factor, as well as the influence of the geometry of ferromagnetic backings on coupling coefficient, was investigated for the system of coils consisting of two identical circular coils. In [23], authors presented an analysis of the impact of coil misalignment on the coupling factor of coreless circular, square, rectangular, and DD coil systems.

As receiver coils are mounted on vehicles in EV charging applications, their design is more demanding, considering weight and volume. A higher freedom for the design of transmission coils could be utilized to achieve higher coupling coefficient and quality factors of the systems. Therefore, such non-symmetrical coil structures could potentially be promising for wireless EV charging applications. This work focuses on an analysis of coil systems with non-symmetrical structures of ferromagnetic backing, compared to conventional, symmetrical ones.

The rest of the paper is organized as follows. An analytical analysis of the coil-to-coil efficiency of the WPT system and the impact of the coupling coefficient on the efficiency is discussed in the following Section 2. The developed FEM model applied for the research and its core implementation details are presented in "Materials and Methods", Section 3. The verification of the model by applying experimental and analytical approaches is given in "Model Verification", Section 4. The obtained results are provided and discussed in the "Results", Section 5. An overview and summary of the results are presented in the "Discussion", Section 6. Conclusions are drawn in the "Conclusions", Section 7.

2. Coupling Coefficient and Efficiency of a WPT System

A WPT system usually is designed and optimized considering its efficiency, power transfer capability, and sensitivity to coil misalignments [14,24,25]. The efficiency is one of the key parameters of a high-power WPT system and can be analyzed analytically according to an equivalent scheme of the WPT system (Figure 1). The equivalent scheme is presented in Figure 2.

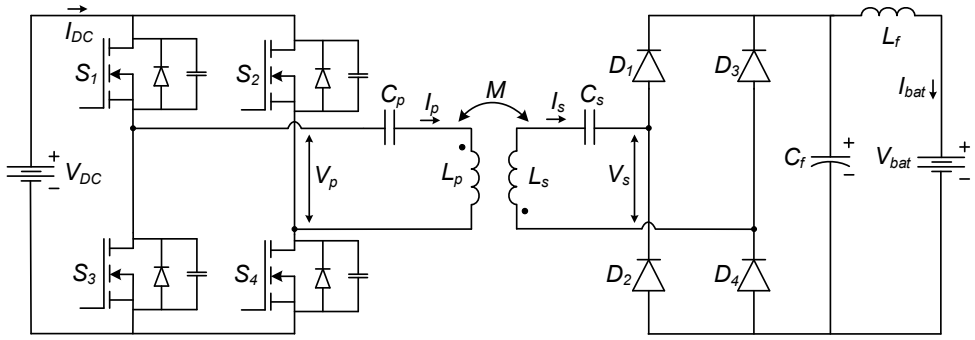

Figure 1. Circuit diagram of a typical Inductive Power Transfer (IPT) system (SS compensation topology).

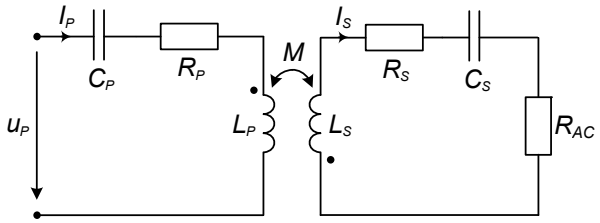

Figure 2. Equivalent scheme of ITP system.

The operation of the circuit is described analytically by the set of equations according Kirchhoff's voltage law:

$$\begin{cases} \boldsymbol{V_p} = \boldsymbol{I_p}\left(\mathrm{j}\omega L_p - \frac{1}{\mathrm{j}\omega C_p} + R_p\right) + \boldsymbol{I_s}\mathrm{j}\omega M, \\ \boldsymbol{V_m} = \boldsymbol{I_s}\left(\mathrm{j}\omega L_s - \frac{1}{\mathrm{j}\omega C_s} + R_s\right) + \boldsymbol{I_s}R_{AC}, \end{cases} \tag{1}$$

where $\boldsymbol{V_p}$ is the primary (source) voltage, $\boldsymbol{I_p}$ and $\boldsymbol{I_s}$ are currents of the primary and secondary coils, $R_p, R_s,\ L_p,\ L_s$ are the resistances and inductances of the primary and secondary coils, $C_p,\ C_s$ are the capacitances of primary and secondary compensation capacitors, respectively, M is the mutual inductance, ω is the angular frequency, and $\boldsymbol{V_m}$ is the voltage induced in the secondary coil $\boldsymbol{V_m} = -\mathrm{j}\omega M\boldsymbol{I_p}$, while R_{AC} is the load resistance, representing the EV battery, seen from the AC side of the secondary (receiving) coil (Figures 1 and 2) [26].

$$R_{AC} = \frac{8}{\pi^2}R_{bat} = \frac{8}{\pi^2} \times \frac{V_{bat}}{I_{bat}}. \tag{2}$$

Coil-to-coil efficiency (the inverter and rectifier losses excluded), expressed from the set of Equation (1) is [27]

$$\eta = \frac{P_L}{P_1} = \frac{\omega^2 M^2 R_{AC}}{R_p\left((R_s + R_{AC})^2 + \left(\omega L_s - \frac{1}{\omega C_s}\right)^2\right) + \omega^2 M^2 (R_s + R_{AC})}. \tag{3}$$

As can be seen from this equation, coil-to-coil efficiency is a complex function of the coils' resistances, secondary side reactance (if not fully compensated), angular frequency, load resistance, and mutual inductance. Considering the relationship of the mutual inductance M and the coupling coefficient k,

$$k = M/\sqrt{L_p L_s}, \tag{4}$$

the efficiency could be expressed as a function of the coupling coefficient:

$$\eta = \frac{P_L}{P_1} = \frac{\omega^2 k^2 L_p L_S R_{AC}}{R_p\left((R_s + R_{AC})^2 + \left(\omega L_s - \frac{1}{\omega C_s}\right)^2\right) + \omega^2 k^2 L_p L_S (R_2 + R_{AC})}. \tag{5}$$

The optimal load is found by differentiation of the expression (5) with respect to R_{AC} when the secondary side inductance is fully compensated $\omega L_s - \frac{1}{\omega C_s} = 0$. The expression of the optimal load resistance is [28]

$$R_{AC,opt} = R_s\sqrt{1 + k^2 Q_p Q_s}, \tag{6}$$

where Q_p and Q_s are the quality factors of the primary and secondary coils, respectively. The maximum achievable coil-to-coil efficiency according to [28] is

$$\eta_{max} = \frac{k^2 Q_p Q_s}{\left(1 + \sqrt{1 + k^2 Q_p Q_s}\right)^2}. \tag{7}$$

The batteries represent the dynamic loads. Therefore, the resistance R_{AC} depends on the operating point of a charging circuit. The DC/DC converters together with control circuits are applied to match the optimal one [29]. They assure the maximum efficiency with respect to the load in the particular state. The maximum achievable coil-to-coil efficiency, corresponding to the optimal load, depends on the coupling coefficient and the quality factors of the coils (7). To achieve the largest efficiency, these parameters must be maximized [30–33].

3. Materials and Methods

The research was carried out by using the finite element method (FEM). COMSOL Multiphysics version 6.1 software was used for the simulations. Three-dimensional geometry was used in the study. It enabled us to develop a comprehensive model and depict geometry in detail. The magnetic field interface was used in the simulations. The interface is based on Maxwell's equations, formulated using the magnetic vector potential [34]. The geometry of the coil systems was implemented in COMSOL directly, using the geometric primitives and geometry operations. A parametrically defined model was developed. It enabled fast and easy manipulations with geometry and allowed us to perform the parametric sweep calculations. The models of the coil systems were encapsulated by an enclosing boundary block, the surface of which was forced to satisfy the magnetic insulation condition. The "Air" material, available in the built-in COMSOL Material library, was used to define properties of the space inside the block, while the "Copper" material was used to define material properties of the coils. The M33 (MnZn) soft ferrite material was chosen for the ferromagnetic backings [20].

The study applied for the simulations consists of two steps. Coil Geometry Analysis is a preprocessing step for the current flow assessment in the 3D model coils. The main step is the frequency domain study w. The excitation frequency used in the study was $f = 85$ kHz. The operation frequency of WPT systems for EV charging applications is determined by Recommended Practice (RP) J2954 of the Automobile Engineers Society (SAE) [35,36]. The nominal operating frequency is $f = 85$ kHz (the tuning band is from 81.38 to 90 kHz).

The list of the main parameters and their values applied in the simulations is presented in Table 1.

Table 1. List and values of the main parameters applied in the simulations.

Parameters, Units	Meaning	Value
R_{out} (cm)	Outer radius of the coils	25
R_{in} (cm)	Inner radius of the coils	11, *
R_{cond} (mm)	Radius of the conductor's cross-sectional area	2.7
N (1)	Number of turns	15, *
l_{gap} (cm)	Air-gap length between the coils	17, *
f (kHz)	Driving frequency	85
h_{fe} (mm)	Thickness of the ferromagnetic plates or bars	8
w_{fe} (cm)	Width of the ferromagnetic bars	2, *
l_{displ} (cm)	Longitudinal displacement of the coils	0, *

* Varies in particular analysis.

4. Model Verification

The accuracy of an FEM model is determined by various factors including the implemented geometry, meshing, boundaries of the model, applied material models, etc. Two approaches for the validation of the developed FEM model were used: comparison with the results obtained by the analytical method and the experimental validation. Both models of the coils (circular and square topologies), without Fe backings, were validated using the analytical approach. The dimensions of the coils in this case were proper for EV charging applications. The experimental approach was used for the validation of the model with the ferrite backings; however, the size of the coils applied in the physical experiment was significantly smaller. Since the parametric approach was used in the FEM model development, it was scaled to these lower dimensions just by adjusting the corresponding parameters, without any additional changes made in the model itself.

The self and mutual inductances of the circular coils (Figure 3) for the analytical verification of the FEM model were calculated using the expressions presented in [37]. The self-inductances of the circular coils were calculated using the numerical form of the following expression [37]:

$$L = \frac{\mu_0}{4\pi} \iint_0^{\Phi} \zeta((a\cos\varphi_1 - y_1)(a\cos\varphi_2 - Y_2) + (a\sin\varphi_1 + x_1)(a\sin\varphi_2 + X_2))d\varphi_1 d\varphi_2, \quad (8)$$

where

$$\zeta = \frac{1}{\sqrt{(X_2 - x_1)^2 + (Y_2 - y_1)^2 + g^2}}, \quad (9)$$

and $a = \delta/(2\pi)$, $\Phi = 2\pi N$, $x_1 = (R_{in} + a\varphi_1)\cos\varphi_1$, $y_1 = (R_{in} + a\varphi_1)\sin\varphi_1$, $X_2 = (R_{in} + a\varphi_2)\cos\varphi_2$, $Y_2 = (R_{in} + a\varphi_2)\sin\varphi_2$, $g = e^{-1/4}R_{cond}$, $\mu_0 = 4\pi{\cdot}10^{-7}$ H/m is magnetic constant, R_{in} is the inner radius of the coil, N is the number of turns, R_{cond} is the radius of the conductor, $\delta = 2R_{cond} + l_{gap}$ is the screw pitch, i.e., distance between the centers of the adjacent turns, and l_{gap} is the air-gap length between the adjacent turns.

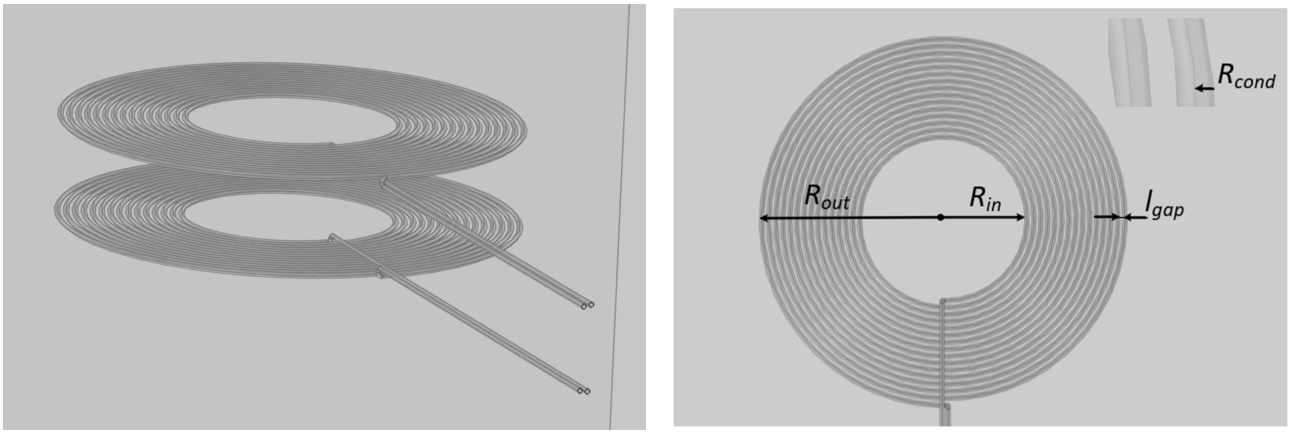

(**a**) (**b**)

Figure 3. FEM model geometry of the planar circular coils: (**a**) geometry for the mutual inductance calculation; (**b**) the main parameters of the coils.

The mutual inductances between the coaxially positioned circular coils, having the same geometrical shape, were calculated using the numerical form of the following expression [37]:

$$M = \frac{\mu_0}{4\pi} \int_0^{\Phi_1} \int_0^{\Phi_2} \chi((a\cos\varphi_1 - y_1)(a\cos\varphi_2 - Y_2) + (a\sin\varphi_1 + x_1)(a\sin\varphi_2 + X_2))d\varphi_1 d\varphi_2, \quad (10)$$

where

$$\chi = \frac{1}{\sqrt{(X_2 - x_1)^2 + (Y_2 - y_1)^2 + h_{air}^2}}, \tag{11}$$

And h_{air} is the distance between the coils.

The comparisons of the results obtained by the developed numerical FEM model and by the analytical expressions (8) and (10) for varying numbers of coil turns are presented in Figure 4. In the verification analysis, the outer radius of the coils was kept constant at $R_{out} = 0.25$ m. The inner radius of the coils R_{in} was recalculated for each case considering the corresponding number of turns N as follows:

$$R_{in} = R_{out} - \left(N2R_{cond} + (N-1)l_{gap}\right). \tag{12}$$

where the conductor diameter $R_{cond} = 2.7$ mm, and the air-gap length between the adjacent turns $l_{gap} = 4$ mm were constant parameters.

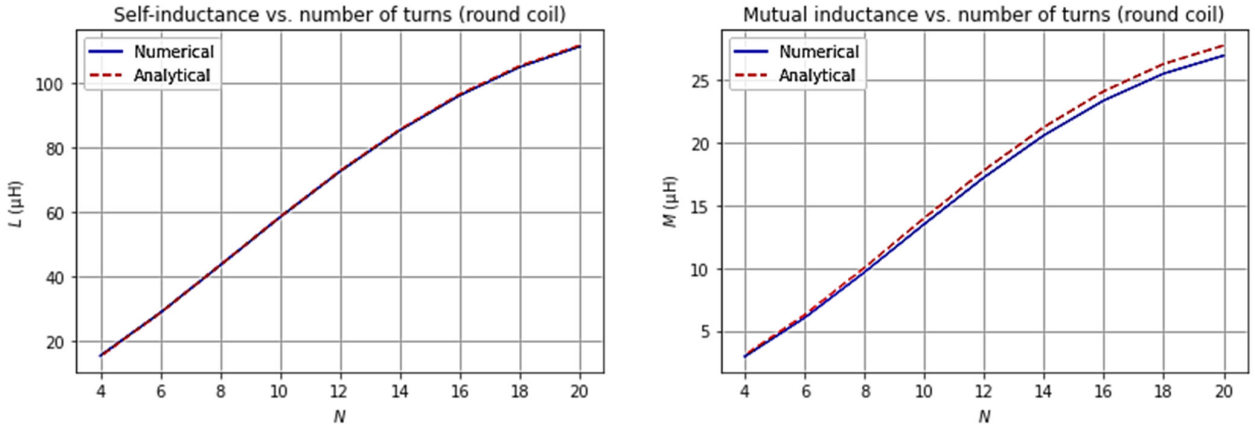

(**a**) (**b**)

Figure 4. Comparison of the circular coil inductances obtained by the FEM model and analytically: (**a**) self-inductance vs. number of turns; (**b**) mutual inductance vs. number of turns ($h_{air} = 15$ cm).

The self and mutual inductances of the square planar coils (Figure 5) were calculated analytically using the expressions presented in [23]. The self-inductances of the square coils were calculated according to the Wheeler formula for square coils [38]:

$$L = 2.34\mu_0 \frac{N^2 d_{avg}}{1 + 2.75\rho'}, \tag{13}$$

where d_{avg} is average diameter of the coil:

$$d_{avg} = R_{in} + R_{out}, \tag{14}$$

and ρ' is the fill ratio:

$$\rho' = \frac{R_{in} - R_{out}}{R_{in} + R_{out}}. \tag{15}$$

The mutual inductance between the coaxially positioned coils of the same geometrical shape were calculated by applying the following expression [23]:

$$M = \frac{2N^2\mu_0}{1 + 2.75\rho'}\left(d_{avg}\ln\left(\frac{d_{avg} + b}{d_{avg} + x} \times \frac{b}{h}\right) + (x - 2b + h)\right), \tag{16}$$

where $b = \left({d_{avg}}^2 + h^2\right)^{1/2}$, and $x = \left(2{d_{avg}}^2 + h^2\right)^{1/2}$.

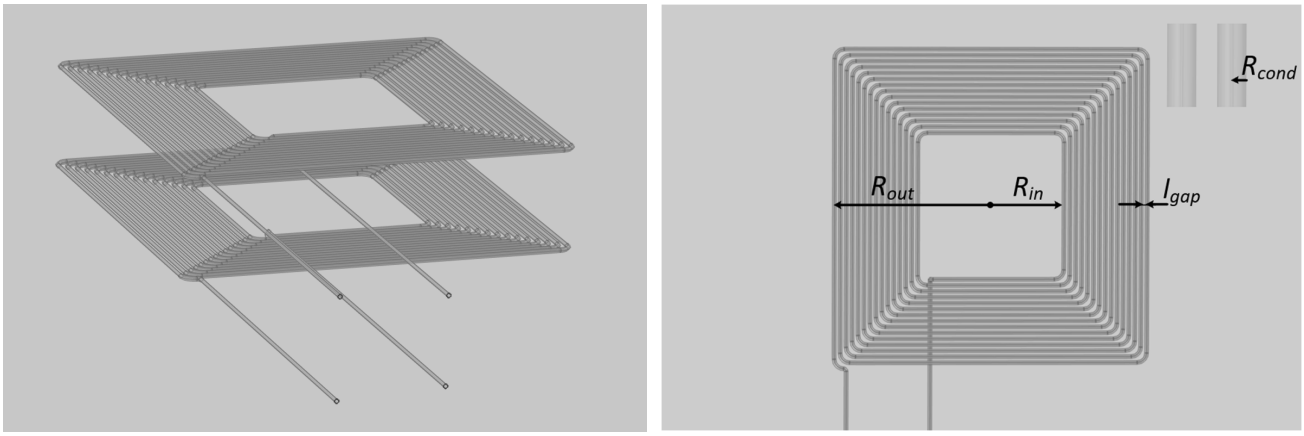

(**a**) (**b**)

Figure 5. FEM model geometry of the planar square coils: (**a**) geometry for the mutual inductance calculation; (**b**) the main parameters of the coils.

The comparison of the results obtained by the numerical FEM model and the analytical calculations obtained by applying (13) and (16) are presented in Figure 6. The results presented in Figures 4 and 6 show the adequacy of the FEM model. The slightly higher differences obtained for the case of the square coils could be explained by the fact that the applied analytical model in this case is less detailed, in comparison to the circular coil case, as the former one does not consider the diameter of the windings.

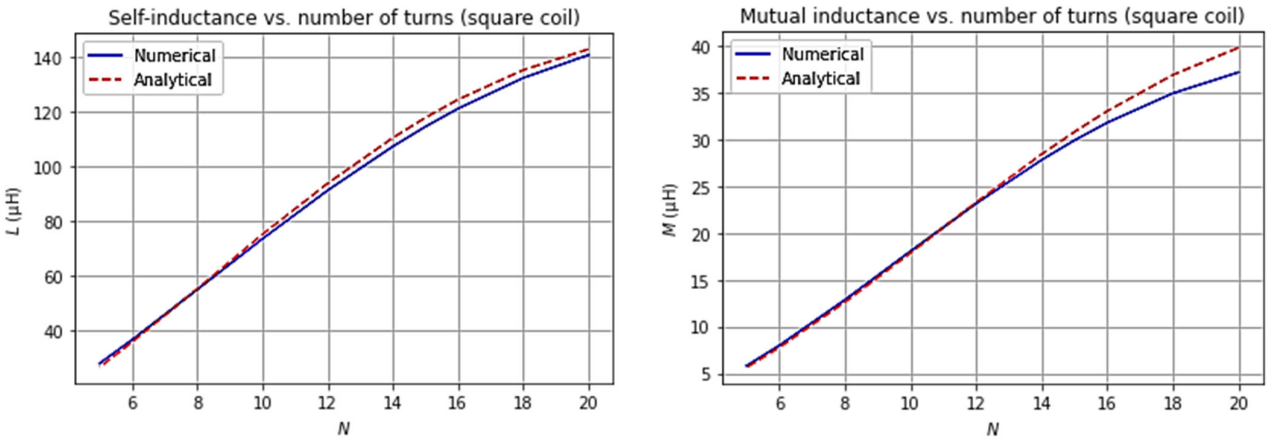

(**a**) (**b**)

Figure 6. Comparison of square coil inductances obtained by the FEM model and analytically: (**a**) self-inductances; (**b**) mutual inductances of the coaxially positioned coils (h_{air} = 15 cm).

The FEM model (Figure 7a) was additionally verified experimentally by applying two identical Würth Elektronik 400 W planar circular wireless power transfer coils [39], in this case with ferrite backings. Experimentally, the values of mutual inductance between the coils were obtained by applying the following procedure. The primary and secondary coils were connected in series at first in aiding and then in opposing ways. The total inductances of the coil system in each case were measured by applying an impedance analyzer. In the aiding case, the total inductance of the coil system could be expressed as the sum of self-inductances of the coils plus double mutual inductance:

$$L'_T = L_p + L_s + 2M, \tag{17}$$

where L_p and L_s are the self-inductances of each coil.

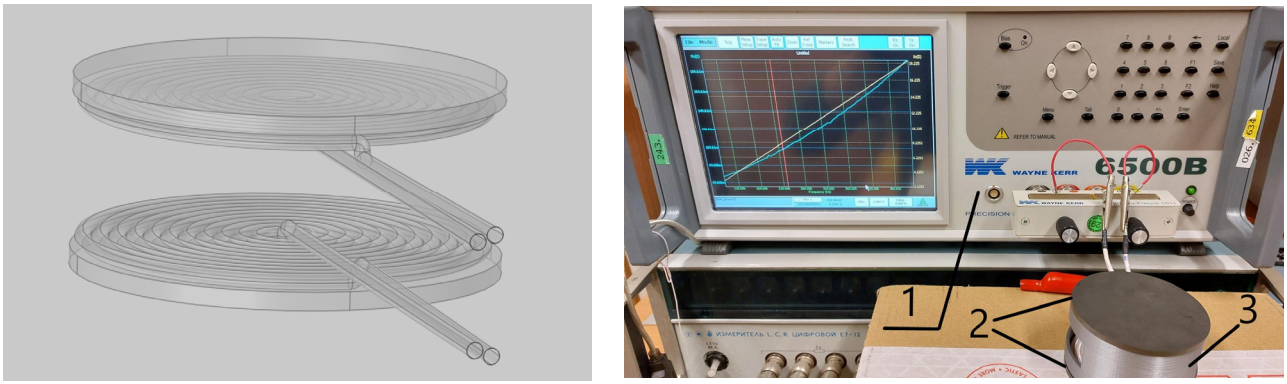

(**a**) (**b**)

Figure 7. (**a**) FEM model geometry of the Würth Elektronik 400 W WPT (Würth Elektronik, Vilnius, Lithuania) coils. (**b**) Experimental setup: (1) impedance analyzer "Wayne Kerr 6500B", (2) coils Würth Elektronik 400 W WPT, (3) coil holder.

In the opposing case, the total inductance of the coil system equals the sum of self-inductances minus double the mutual inductance:

$$L_T'' = L_p + L_s - 2M. \tag{18}$$

The mutual inductance could be expressed by subtracting (18) from (17) and leads to the following expression:

$$M = \frac{L_T' - L_T''}{4}, \tag{19}$$

which was applied for the experimentally obtained mutual inductance calculation. The comparison of the results obtained by the FEM model and experimentally is presented in Table 2.

Table 2. Comparison of the results obtained by the FEM model and the results obtained experimentally.

Air-Gap (cm)	*M* (μH) FEM Results	*M* (μH) Experimental Results	Error
2	1.70	1.72	1.54 (%)
3	0.903	0.925	2.31 (%)
4	0.509	0.532	4.34 (%)
5	0.308	0.324	4.97 (%)

The "Wayne Kerr 6500B" (Wayne Kerr Europe GmbH, Iserlohn, Germany) impedance analyzer was used for the measurement of the inductances. A view of the applied experimental setup is presented in Figure 7b. To assure the particular required distance between the coils, coil holders made by a 3D printer were used.

The physical experiment, as well as the analytical verification, confirmed the adequacy of the FEM model.

5. Results

It is well-known that ferromagnetic (ferrite) cores or backings are often used in designs of coil systems to maximize the coupling between the coils. The coil systems for WPT are no exception. The impact of the ferrite backing design on the coupling coefficient of the WPT coils was investigated in this study. The conventional, symmetrical systems without ferrites, with the planar ferrite cores, the cores made from ferrite bars, and the non-conventional, asymmetrical systems were considered. The latter structures are potentially beneficial for automotive applications, because of the different requirements for each coil of the system. A minimization of the weight and size of the coil mounted on vehicle is crucial, while the

stationary case is less demanding in the latter sense. We investigated two types of such coil systems with non-symmetrical structures. The first one consists of one coil with a planar ferrite backing, and the second coil lacks a ferrite backing (Figure 8). The second investigated structure consists of one coil having a planar ferrite backing and the second coil having a backing made from ferrite bars (Figure 9). The symmetrical coil structures with ferromagnetic bars (Figure 10), with ferromagnetic plates (Figure 11), and without any ferromagnetic cores (Figure 12) were analyzed as well. Two geometries of the coils, circular and square, with the mentioned core structures were investigated.

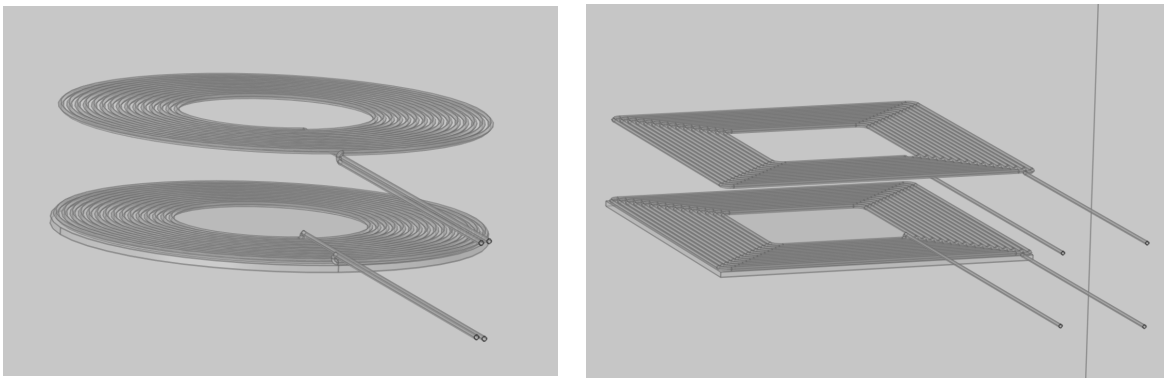

(**a**) (**b**)

Figure 8. Geometries of the coils with non-symmetrical Fe backing structure: one coil with ferrite plate using (**a**) circular coils; (**b**) square coils.

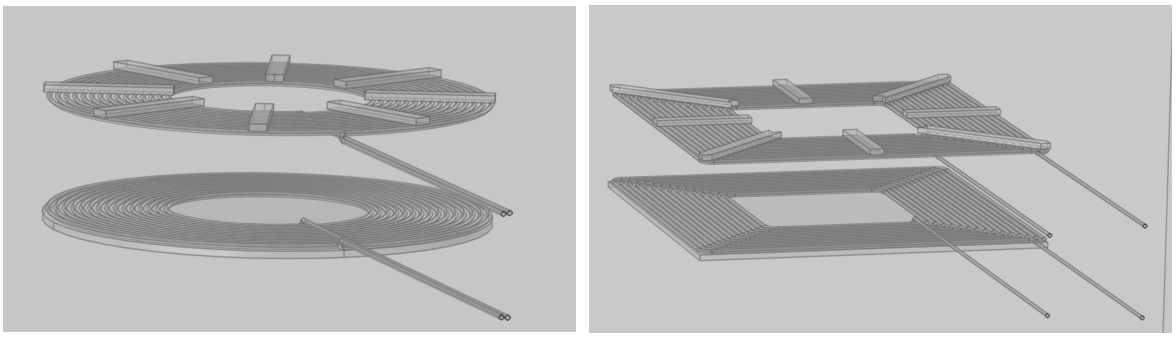

(**a**) (**b**)

Figure 9. Geometries of the coils with non-symmetrical Fe backing structure: one coil with ferrite plate, one with ferrite bars using (**a**) circular coils; (**b**) square coils.

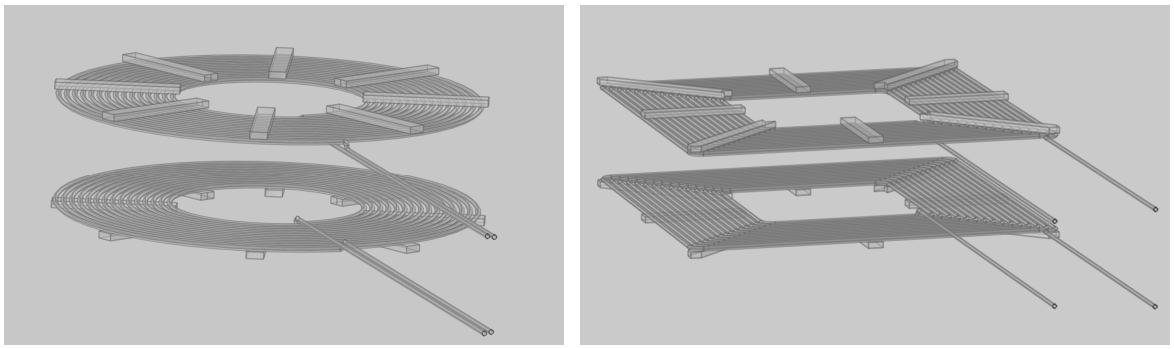

(**a**) (**b**)

Figure 10. Geometries of the coils with symmetrical Fe backing structure: both coils with ferrite bars using (**a**) circular coils; (**b**) square coils.

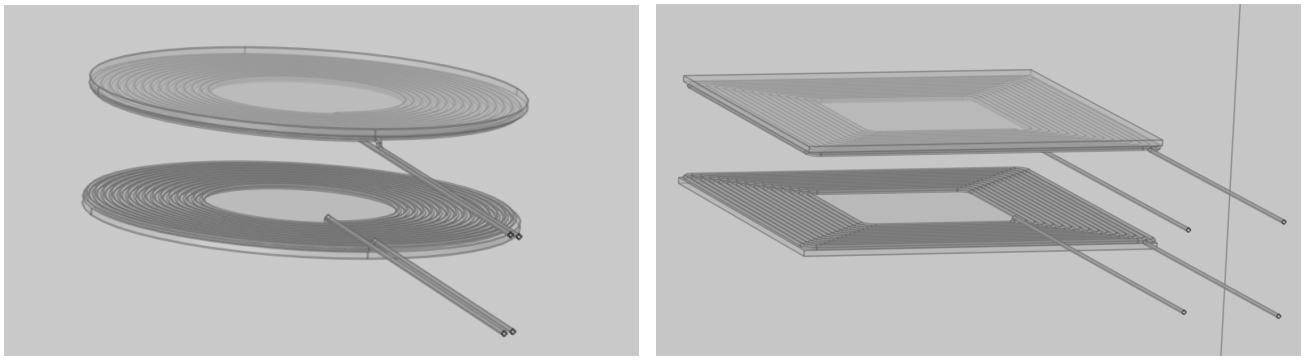

(**a**) (**b**)

Figure 11. Geometry of the coils with symmetrical Fe backing structure: both coils with ferrite plates using (**a**) circular coils; (**b**) square coils.

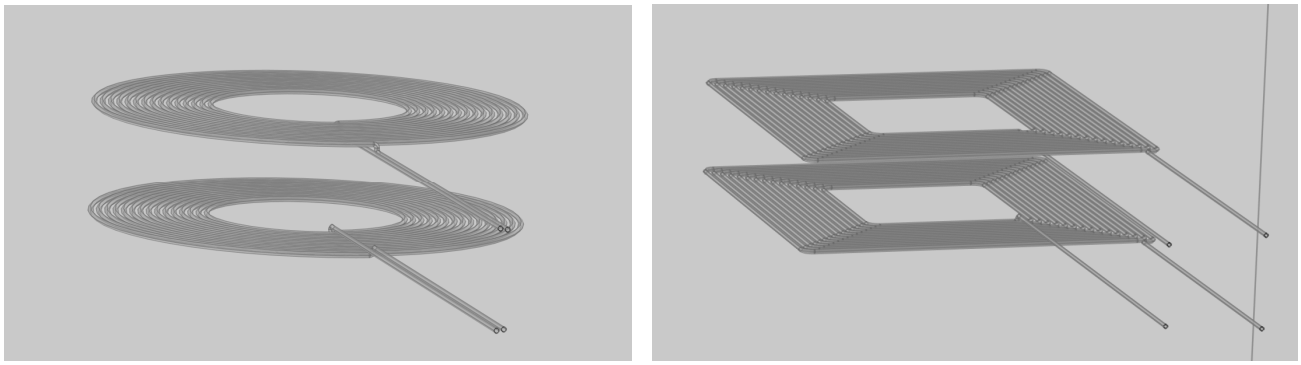

(**a**) (**b**)

Figure 12. Geometry of the coils with symmetrical Fe backing structure: both coils without ferrite backings using (**a**) circular coils; (**b**) square coils.

5.1. Impact of Air-Gap Length on Coupling Coefficient

The FEM simulations were accomplished for different air-gap lengths in the range of 10 ÷ 25 cm, which encompass Z Class 1 ÷ Z Class 3 classes according to SAE J2954 [35]. The results for the coil systems having circular and square geometries are presented in Figure 13a and Figure 13b, respectively.

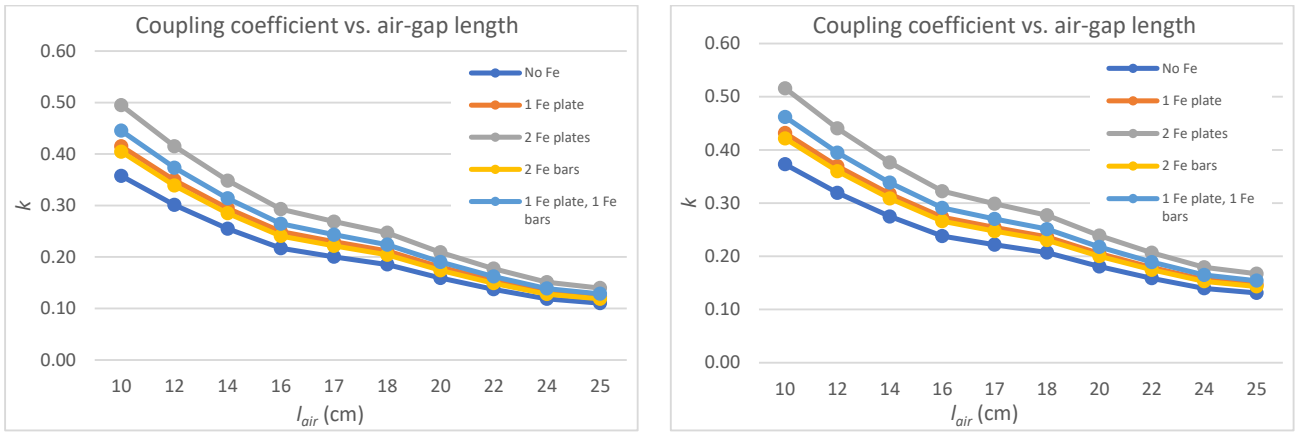

(**a**) (**b**)

Figure 13. Coupling coefficient vs. air-gap length: (**a**) circular coils; (**b**) square coils.

The results indicate that the dependencies of the coupling coefficient vs. air-gap length for both circular and square coil systems have similar pattern, but the square coil systems show a slight superiority over the circular ones. The structures of the coils with cores having higher ferromagnetic volume produce the higher coupling coefficient values. However, it comes with the price of increased weight, space, and cost of the system. The structure composed of one coil with a ferrite plate and one coil with ferrite bars looks promising for vehicle charging applications.

5.2. Impact of Longitudinal Displacement on Coupling Coefficient for Different Structures of the Cores

The simulations were performed for the case of the air-gap length of 17 cm, which corresponds to an average ground clearance of a compact sedan of 17 cm and is close to the average clearance of a typical sedan (16.5 cm) or a hatchback (16.8 cm). The other parameters of the coils (Figure 14) are presented in Table 1. The results are presented in Figure 15.

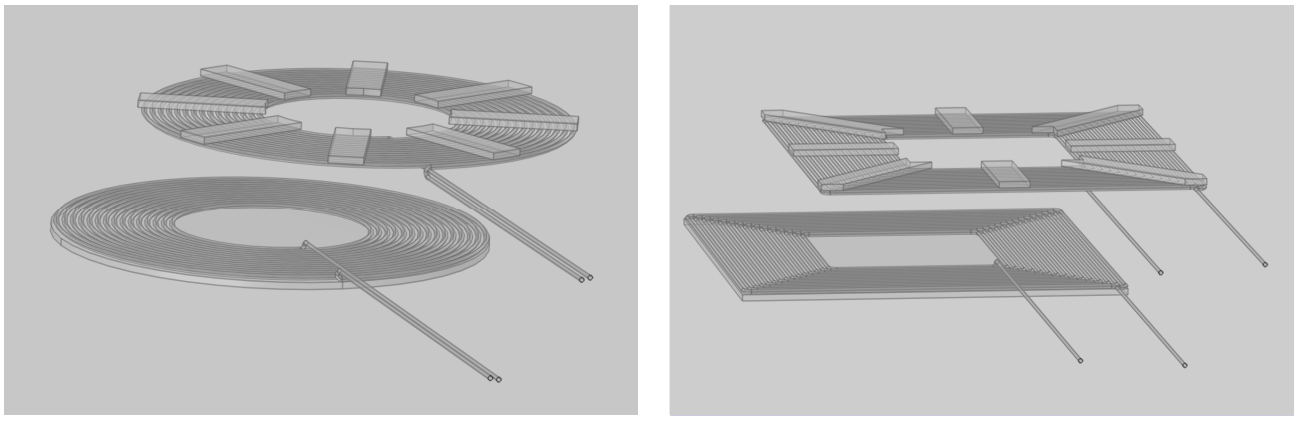

(**a**) (**b**)

Figure 14. Coils with longitudinal displacement: (**a**) circular coils; (**b**) square coils.

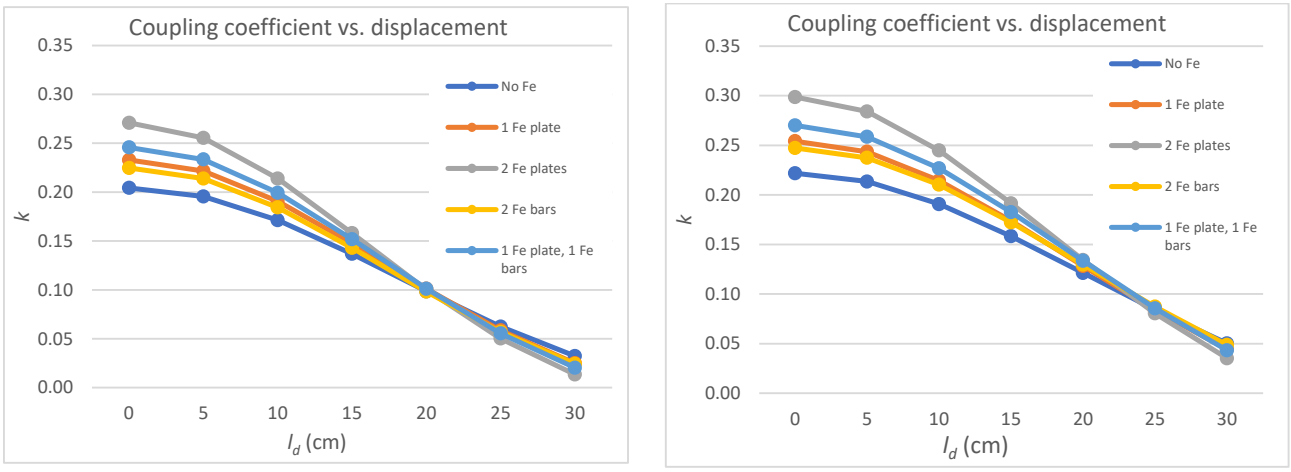

(**a**) (**b**)

Figure 15. Coupling coefficient vs. longitudinal displacement: (**a**) circular coils; (**b**) square coils.

The results show that the coil structures having cores with higher volume or ferrite exhibit higher sensitivity to the horizontal displacement. It is valid for both circular and square-type coils. At the particular displacement, coils with the cores having higher volume

of ferrite produce lower coupling coefficient values. Again, here the coil structures having square-type geometry show superiority over the circular ones.

5.3. Impact of Number of Turns on Coupling Coefficient for Different Structures of the Cores

The simulations were performed for the case of the air-gap length of 17 cm. The other parameters of the coils (Figure 16) are presented in Table 1. The results are presented in Figure 17.

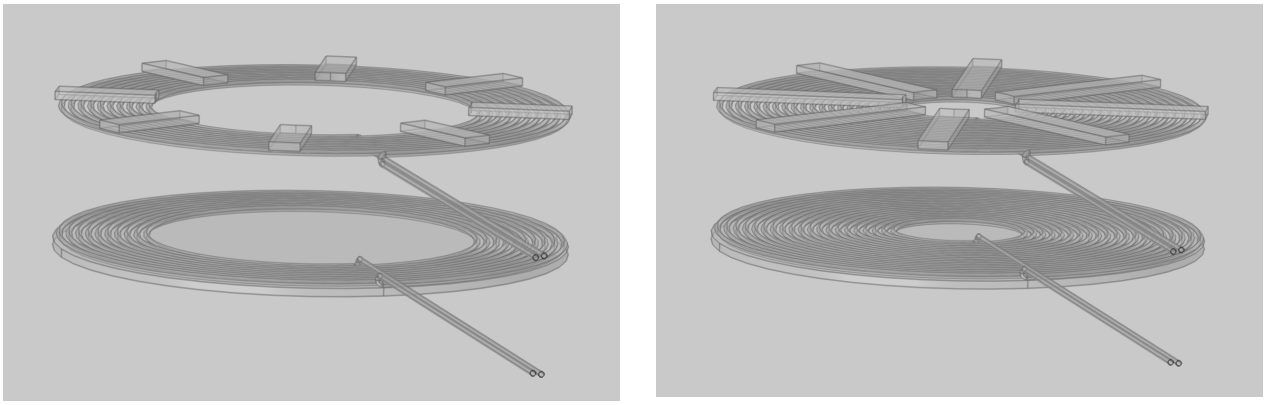

(**a**) (**b**)

Figure 16. Geometries of the circular coils: (**a**) with 10 turns; (**b**) with 20 turns.

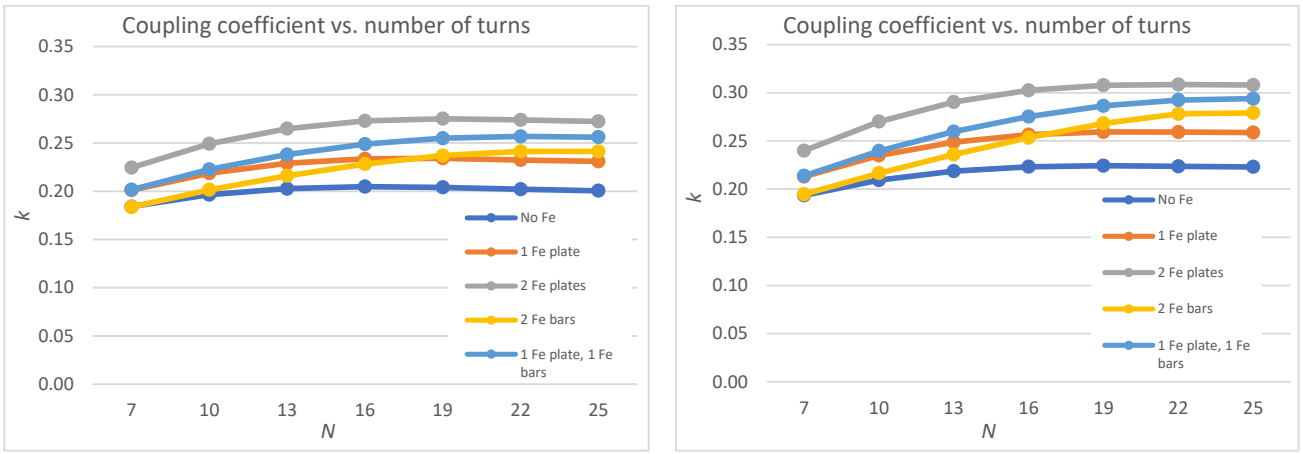

(**a**) (**b**)

Figure 17. Coupling coefficient vs. number of turns: (**a**) circular coils; (**b**) square coils.

The results show that the higher number of turns determines the higher coupling coefficient values just in the lower range of the number of turns. From a particular point, the increase in the number of turns does not produce growth of the coupling coefficient. The highest sensitivity here shows the coil structures with ferrite bars for both circular and square-type geometry cases.

5.4. Impact of Width of the Ferrite Bars on Coupling Coefficient of Coil Systems with Bar–Plate Core Structure

The simulations were performed for the case of the air-gap length of 17 cm. The other parameters of the coils (Figure 18) are presented in Table 1. The results are presented in Figure 19.

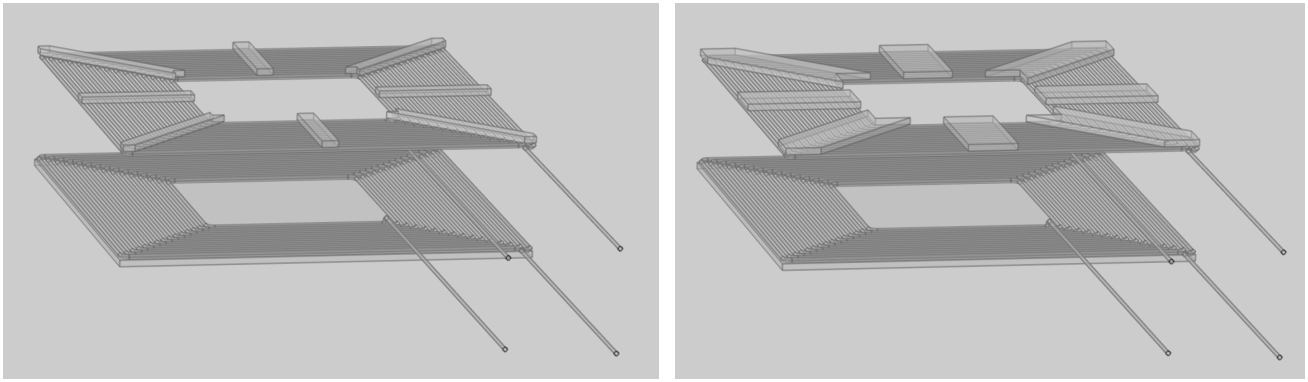

(**a**) (**b**)

Figure 18. Geometry of the square coils: (**a**) width of the Fe bars 2 cm; (**b**) width of the Fe bars 4 cm.

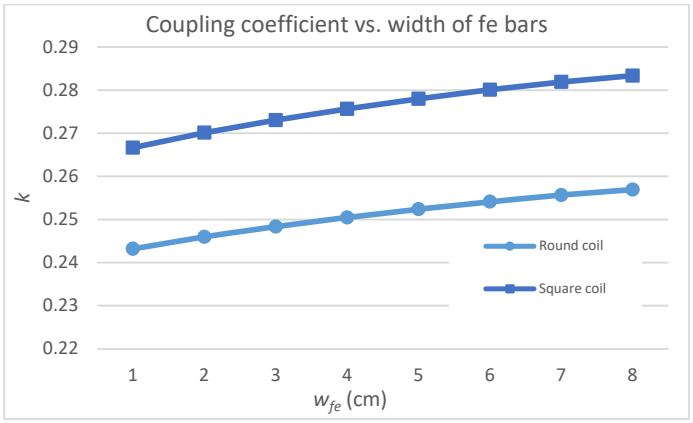

Figure 19. Coupling coefficient vs. width of the ferromagnetic bars.

The results show that the dependencies of the coupling coefficient vs. width of the bars have a nearly linear relationship in the considered range. It is valid for both circular and square-type geometries. Predictably, the higher coupling coefficient values are produced by the coil structures which have backings with higher ferrite volume.

6. Discussion

The results show that the dependencies of the coupling coefficient vs. air-gap length of the coils having both circular and square geometries have similar pattern. The structures of the coils with cores having higher ferromagnetic volume (ferrite) show superiority considering the coupling coefficient. The results of the investigation of the impact of longitudinal coil displacement show that the coil structures which have cores with a higher volume of ferrite show higher sensitivity to the displacement, and from a particular range of the displacement, even produce lower values of the coupling coefficient. The research of the impact of the number of turns on the coupling coefficient shows that an increased number of turns causes higher values of the coupling coefficient only in the lower range of the number of turns. From a particular point, the increase in the number of turns does not cause growth of the coupling coefficient. The highest sensitivity is exhibited by the structures with backings having ferromagnetic bars. The impact of the width of the ferromagnetic bars on the coupling coefficient shows nearly linear dependencies in the investigated range. Predictably, the higher coupling coefficient values are produced by the coils having higher volume of the ferromagnetic backings. In all the considered cases, the coil systems having square geometry showed noticeable superiority over the circular ones with respect to the coupling coefficient value.

7. Conclusions

The rapid growth of electric vehicles on the roads demands proper attention to the development of the charging infrastructure. Significant attention of scientists and industry is paid to the development, optimization, and adaptation of wireless power transfer technology for EV charging applications. Due to its benefits, such as convenience, safety, and reliability, wireless charging has been recently seen as reasonably complementary to AC and DC conductive charging for automotive applications. Many studies have been performed for the analysis and optimization of whole WPT systems or their components. The analysis of the coil systems is no exception; however, there is a lack of knowledge about the properties of coil systems having different realizations of the ferrite elements for the transmitter and receiver coils. Such coil systems for EV charging applications could be beneficial because they enable the minimization of the weight and size of the on-board coil. The analysis of such coil systems is presented in this work. The results of the research imply that the coil systems having non-symmetrical structures of the ferromagnetic backings could be a good alternative to the conventional symmetrical approaches for wireless electrical vehicle charging applications. They provide reasonable values of the coupling coefficient with reduced weight and size of the coils mounted on a vehicle. The compromise between the weight, size of the coil mounted on the vehicle, and the coupling coefficient of the coil system for a particular case could be achieved by varying the width of the bars in the plate–bar backing structure.

The focus of this work was set on the analysis of the coil assemblies of spiral circular and spiral square shapes. However, coils having other topologies, like double D (DD) and DD-quadrature (DDQ), have characteristics beneficial for EV charging, especially in dynamic wireless charging applications. Therefore, future work will target an analysis of coil systems of the mentioned topologies with non-symmetrical Fe backings.

Author Contributions: Conceptualization, R.L. and Ž.N.; methodology, R.L. and A.V.; software, R.L.; validation, R.L., R.D., Ž.N. and A.V.; formal analysis, R.L.; investigation, R.L. and R.D.; resources, R.L., A.V. and Ž.N.; data curation, R.L., R.D. and L.R.; writing—original draft preparation, R.L.; writing—review and editing, R.L., R.D., Ž.N., A.V. and L.R.; visualization, R.L., R.D. and L.R. All authors have read and agreed to the published version of the manuscript.

Funding: This research received no external funding.

Institutional Review Board Statement: Not applicable.

Informed Consent Statement: Not applicable.

Data Availability Statement: The data underlying the results presented in this paper are not publicly available at this time but may be obtained from the authors upon reasonable request.

Acknowledgments: The authors would like to express their gratitude to a student at Kaunas University of Technology, Matas Agliniškis, for help with experimental setup and experimental data acquisition.

Conflicts of Interest: The authors declare no conflicts of interest.

References

1. SNS Insider. Available online: https://www.snsinsider.com/reports/wireless-charging-market-1361 (accessed on 15 November 2023).
2. Detka, K.; Górecki, K. Wireless Power Transfer—A Review. *Energies* **2022**, *15*, 7236. [CrossRef]
3. Cheong, Y.; Cao, S.; Naayagi, R.T.; Lee, S. Triple Phase Shift Control of Wireless Charging DAB LCC Resonant Converter for Unity Power Factor Operation with Optimized Rectifier AC Load Resistance. *Appl. Sci.* **2022**, *12*, 11871. [CrossRef]
4. Arnaudov, D.D.; Madzharov, N.D.; Hinov, N.L. Rotary Wireless Inductive Transmitter Powered by ZVS Resonant Convertor. *Elektron. Elektrotechn.* **2019**, *25*, 17. [CrossRef]
5. Feng, H.; Tavakoli, R.; Onar, O.C.; Pantic, Z. Advances in High-Power Wireless Charging Systems: Overview and Design. *Consid. IEEE Trans. Transp. Electrif.* **2020**, *6*, 886. [CrossRef]
6. Skorvaga, J.; Frivaldsky, M.; Pavelek, M. Design of a Wireless Charging System for e-Scooter. *Elektron. Elektrotechn.* **2021**, *27*, 40. [CrossRef]

7. Fenton, D.; Kailas, A. Redefining Goods Movement: Building an Ecosystem for the Introduction of Heavy-Duty Battery-Electric Vehicles. *World Electr. Veh. J.* **2021**, *12*, 147. [CrossRef]
8. Mohamed, N.; Aymen, F.; Alqarni, M.; Turky, R.A.; Alamri, B.; Ali, Z.M.; Aleem, S.H.A. A new wireless charging system for electric vehicles using two receiver coils. *Ain Shams Eng. J.* **2022**, *13*, 101569. [CrossRef]
9. Kakkar, R.; Gupta, R.; Agrawal, S.; Tanwar, S.; Sharma, R.; Alkhayyat, A.; Neagu, B.-C.; Raboaca, M.S. A Review on Standardizing Electric Vehicles Community Charging Service Operator Infrastructure. *Appl. Sci.* **2022**, *12*, 12096. [CrossRef]
10. Taghizad-Tavana, K.; Alizadeh, A.; Ghanbari-Ghalehjoughi, M.; Nojavan, S. A Comprehensive Review of Electric Vehicles in Energy Systems: Integration with Renewable Energy Sources, Charging Levels, Different Types, and Standards. *Energies* **2023**, *16*, 630. [CrossRef]
11. Nordström, H.; Söder, L.; Flynn, D.; Matevosyan, J.; Kiviluoma, J.; Holttinen, H.; Vrana, T.K.; van der Welle, A.; Morales-España, G.; Pudjianto, D.; et al. Strategies for Continuous Balancing in Future Power Systems with High Wind and Solar Shares. *Energies* **2023**, *16*, 5249. [CrossRef]
12. Bellocchi, S.; Klöckner, K.; Manno, M.; Noussan, M.; Vellini, M. On the role of electric vehicles towards low-carbon energy systems: Italy and Germany in comparison. *Appl. Energy* **2019**, *255*, 113848. [CrossRef]
13. Lim, K.L.; Speidel, S.; Bräunl, T. A comparative study of AC and DC public electric vehicle charging station usage in Western Australia. *Renew. Sustain. Energy Transit.* **2022**, *2*, 100021. [CrossRef]
14. Li, G.; Jo, C.-H.; Shin, C.-S.; Jo, S.; Kim, D.-H. A Load-Independent Current/Voltage IPT Charger with Secondary Side-Controlled Hybrid-Compensated Topology for Electric Vehicles. *Appl. Sci.* **2022**, *12*, 10899. [CrossRef]
15. Jo, S.; Shin, C.-S.; Kim, D.-H. Novel Design Method in Wireless Charger for SS Topology with Current/Voltage Self-Limitation Function. *Appl. Sci.* **2023**, *13*, 1488. [CrossRef]
16. Ghazizadeh, S.; Ahmed, K.; Seyedmahmoudian, M.; Mekhilef, S.; Chandran, J.; Stojcevski, A. Critical Analysis of Simulation of Misalignment in Wireless Charging of Electric Vehicles Batteries. *Batteries* **2023**, *9*, 106. [CrossRef]
17. Van Mulders, J.; Delabie, D.; Lecluyse, C.; Buyle, C.; Callebaut, G.; Van der Perre, L.; De Strycker, L. Wireless Power Transfer: Systems, Circuits, Standards, and Use Cases. *Sensors* **2022**, *22*, 5573. [CrossRef]
18. Yakala, R.K.; Pramanick, S.; Nayak, D.P. Optimization of Circular Coil Design for Wireless Power Transfer System in Electric Vehicle Battery Charging Applications. *Trans. Indian Natl. Acad. Eng.* **2021**, *6*, 765–774. [CrossRef]
19. Nakutis, Ž.; Lukočius, R.; Girdenis, V.; Kroičs, K. A Measurement Method of Power Transferred to an Electric Vehicle Using Wireless Charging. *Sensors* **2023**, *23*, 9636. [CrossRef] [PubMed]
20. Corti, F.; Grasso, F.; Paolucci, L.; Pugi, L.; Luchetti, L. Circular Coil for EV Wireless Charging Design and Optimization Considering Ferrite Saturation. In Proceedings of the 2019 IEEE 5th International forum on Research and Technology for Society and Industry (RTSI), Florence, Italy, 9–12 September 2019; pp. 279–284. [CrossRef]
21. Ongayo, D.; Hanif, M. Comparison of circular and rectangular coil transformer parameters for wireless Power Transfer based on Finite Element Analysis. In Proceedings of the 2015 IEEE 13th Brazilian Power Electronics Conference and 1st Southern Power Electronics Conference (COBEP/SPEC), Fortaleza, Brazil, 29 November–2 December 2015; pp. 1–6. [CrossRef]
22. Moghaddami, M.; Anzalchi, A.; Sarwat, A.I. Finite element based design optimization of magnetic structures for roadway inductive power transfer systems. In Proceedings of the 2016 IEEE Transportation Electrification Conference and Expo (ITEC), Dearborn, MI, USA, 27–29 June 2016; pp. 1–6. [CrossRef]
23. Yang, Y.; Cui, J.; Cui, X. Design and Analysis of Magnetic Coils for Optimizing the Coupling Coefficient in an Electric Vehicle Wireless Power Transfer System. *Energies* **2020**, *13*, 4143. [CrossRef]
24. Li, S.; Yang, F.; Huang, Y.; Zhao, H. Comprehensive investigation on misalignment tolerance of inductive power transfer systems. *Energy Rep.* **2023**, *9*, 1578. [CrossRef]
25. Leng, Y.; Luo, D.; Li, Z.; Yu, F. Coupling coefficient calculation and optimization of positive rectangular series coils in wireless power transfer systems. *Heliyon* **2023**, *9*, e21121. [CrossRef] [PubMed]
26. Capua, G.; Femia, N. Optimal Coils and Control Matching in Wireless Power Transfer Dynamic Battery Chargers for Electric Vehicles. *IEEE Access* **2021**, *9*, 166542. [CrossRef]
27. Huang, Z.; Wong, S.-C.; Tse, C.K. Design of a Single-Stage Inductive-Power-Transfer Converter for Efficient EV Battery Charging. *IEEE Trans. Veh. Technol.* **2017**, *66*, 5808–5821. [CrossRef]
28. Zhang, Z.; Pang, H.; Georgiadis, A.; Cecati, C. Wireless Power Transfer—An Overview. *IEEE Trans. Ind. Electron.* **2019**, *66*, 1044–1058. [CrossRef]
29. Laha, A.; Kalathy, A.; Pahlevani, M.; Jain, P. A Comprehensive Review on Wireless Power Transfer Systems for Charging Portable Electronics. *Eng* **2023**, *4*, 1023–1057. [CrossRef]
30. Ghadeer, S.; Rezaei-Hosseinabadi, N.; Tabesh, A.; Khajehoddin, S.A. Improving Wireless Power Transfer Efficiency Considering Rectifier Input Impedance and Load Quality Factor. *IEEE Access* **2023**, *11*, 61738. [CrossRef]
31. Li, S.; Mi, C.C. Wireless Power Transfer for Electric Vehicle Applications. *IEEE J. Emerg. Sel. Top. Power Electron.* **2015**, *3*, 4. [CrossRef]
32. Onar, O.C.; Chinthavali, M.; Campbell, S.L.; Seiber, L.E.; White, C.P.; Galigekere, V.P. Modeling, Simulation, and Experimental Verification of a 20-kW Series-Series Wireless Power Transfer System for a Toyota RAV4 Electric Vehicle. In Proceedings of the IEEE Transportation Electrification Conference and Expo (ITEC), Long Beach, CA, USA, 13–15 June 2018; p. 874. [CrossRef]

33. Chatterjee, S.; Iyer, A.; Bharatiraja, C.; Vaghasia, I.; Rajesh, V. Design Optimisation for an Efficient Wireless Power Transfer System for Electric Vehicles. *Energy Procedia* **2017**, *117*, 1015. [CrossRef]
34. The AC/DC Module User's Guide—COMSOL Documentation. Available online: https://doc.comsol.com/5.4/doc/com.comsol.help.acdc/ACDCModuleUsersGuide.pdf (accessed on 15 November 2023).
35. SAE International | Standards | J2954_202010. Available online: https://www.sae.org/standards/content/j2954_202010/ (accessed on 27 December 2023).
36. Campi, T.; Cruciani, S.; Maradei, F.; Feliziani, M. Magnetic Field during Wireless Charging in an Electric Vehicle According to Standard SAE J2954. *Energies* **2019**, *12*, 1795. [CrossRef]
37. Liu, S.; Su, J.; Lai, J.; Zhang, J.; Xu, H. Precise Modeling of Mutual Inductance for Planar Spiral Coils in Wireless Power Transfer and Its Application. *IEEE Trans. Power Electron.* **2021**, *36*, 9876. [CrossRef]
38. Mohan, S.S.; Hershenson, M.D.; Boyd, S.P.; Lee, T. Simple accurate expressions for planar spiral inductances. *IEEE J. Solid. State Circuits* **1999**, *34*, 1419. Available online: https://api.semanticscholar.org/CorpusID:14604387 (accessed on 27 December 2023). [CrossRef]
39. Würth Elektronik | Transfer Transmitter Coil. ORDER CODE. 760308101311 Documentation. Available online: https://www.we-online.com/components/products/datasheet/760308101311.pdf (accessed on 15 November 2023).